

When does atomic resolution plan view imaging of surfaces work?



Pratik Koirala^a, Yuyuan Lin^a, Jim Ciston^b, Laurence D. Marks^{a,*}

^a Department of Materials Science and Engineering, Northwestern University, Evanston, IL 60208, USA

^b National Center for Electron Microscopy, The Molecular Foundry, Lawrence Berkeley National Laboratory, Berkeley, CA 94720, USA

ARTICLE INFO

Article history:

Received 6 April 2016

Received in revised form

7 July 2016

Accepted 5 August 2016

Available online 6 August 2016

Keywords:

Transmission electron microscopy

Plan view imaging

Surface reconstruction

ABSTRACT

Surface structures that are different from the corresponding bulk, reconstructions, are exceedingly difficult to characterize with most experimental methods. Scanning tunneling microscopy, the workhorse for imaging complex surface structures of metals and semiconductors, is not as effective for oxides and other insulating materials. This paper details the use of transmission electron microscopy plan view imaging in conjunction with image processing for solving complex surface structures. We address the issue of extracting the surface structure from a weak signal with a large bulk contribution. This method requires the sample to be thin enough for kinematical assumptions to be valid. The analysis was performed on two sets of data, $c(6 \times 2)$ on the (100) surface and (3×3) on the (111) surface of SrTiO₃, and was unsuccessful in the latter due to the thickness of the sample and a lack of inversion symmetry. The limits and the functionality of this method are discussed.

© 2016 Elsevier B.V. All rights reserved.

1. Introduction

The challenge of extracting a signal with low intensity from a projection with other strong signals has always been pertinent to the field of signal processing. A similar challenge exists in the surface science community to extract the surface structure from one with a large bulk component. Several techniques have been developed both from the theoretical and experimental fronts to address this issue. For conducting materials and simple unit cells, low-energy electron diffraction (LEED) is a very powerful approach [1–6], particularly when complemented by atomic resolution scanning probe methods [4,7–23]. Transmission electron diffraction (TED) [24,25] in unison with direct methods [26–29], X-ray scattering studies [29–31], reflection high energy electron diffraction (RHEED) [20,32,33] and recently high resolution secondary electron microscopy (HRSEM) [34] have also been effectively used to study surface structures. In many cases, these methods are complementary.

With more complex reconstructions and also insulators, many of these techniques have very severe limitations. This is particularly relevant for oxide materials which have an abundance of surface reconstructions; even the prototypical perovskite material SrTiO₃ has highly complex surface structures [1,2,4,6,9,12–14,16,17,19,21–25,27,29,34–37]. The surfaces of these oxides are of

prime importance as many phenomena occur at the surface. For instance, the 2D electron gas [38,39] at the LaAlO₃/SrTiO₃ interface is a direct consequence of the interfacial structures of the two oxides. This paper presents plan view high resolution transmission electron microscopy as a viable approach for imaging complex surface structures and the complexities therein.

Transmission electron microscopy (TEM) is a powerful technique for studying complex surfaces due to its high signal to noise ratio. TEM is used in two different modes, plan view [40–50] and profile view [48,49,51–71], with respect to the orientation of the sample surface. Imaging of nanoparticle surfaces is more suited to profile view imaging as has been demonstrated for gold and silver particles [51–63] and more recently for oxide nanoparticles [72,73]. It can give out of plane relaxations but includes little to no information along the beam direction. On the other hand, plan view imaging provides two-dimensional information in the plane of the surface, although no information normal to the surface, and has been previously used to solve two highly complex surface reconstruction [34,41].

In plan view one has surface structures on both top and bottom surfaces, and must extract the single surface information to move forward. The approach used to date is to assume a kinematical model and linear imaging theory, and consider the image after bulk removal to be a simple addition of the top and bottom surface [41] as:

$$\Psi(\mathbf{r})=1+\sigma[V(\mathbf{r})+V(\mathbf{d}-\mathbf{r})]$$

* Corresponding author.

E-mail address: l-marks@northwestern.edu (L.D. Marks).

$$I(\mathbf{r}) = 1 + \int \sigma T(\mathbf{u}) \{ V(\mathbf{u}) + V^*(\mathbf{u}) \exp(2\pi i \mathbf{d} \cdot \mathbf{u}) \} \times \exp(-2\pi i \mathbf{u} \cdot \mathbf{r}) d\mathbf{u} + \eta(\mathbf{r})$$

where, $V(\mathbf{r})$ and $V(\mathbf{d}-\mathbf{r})$ are the potentials of the top and bottom surfaces respectively, \mathbf{d} is the in plane translation vector between the top and bottom surfaces, σ is the relativistic interaction constant, $T(\mathbf{u})$ accounts for the microscope parameters and $\eta(\mathbf{r})$ is the noise in the image. For completeness, we note that without the bulk component this is not a true “image” of the surface, rather a surface sensitive difference closer to a difference map in a conventional crystallographic sense. One deals with the same type of signal when using direct methods for surfaces, and the loss of the bulk component in general has not proved to be an issue in interpreting the maps [26–29,74].

While this method can work [34,41], it ignores dynamical diffraction coupling with the bulk (e.g. [44,47,50,75–77]) and the limitations and functionality of this method have not been analyzed in detail to date. In this paper, we discuss this in more detail, showing that the method is only robust when the surface contains inversion symmetry.

2. Methods

2.1. Sample preparation

Self-supported single crystal samples were prepared from bulk (100) and (111) SrTiO₃ substrates purchased from MTI Corporation (Richmond, CA). They were cut into 3 mm discs using an ultrasonic cutter, mechanically thinned to a thickness of ~100 μm using silicon carbide sandpaper, then dimpled with a Gatan 656 Dimple Grinder and 0.5 μm diamond slurry until the thickness at the center was ~30 μm. The samples were then washed with de-ionized water, soaked in acetone overnight and finally cleaned with methanol. The samples were then Ar⁺ ion milled to electron transparency using a Gatan Precision Ion Polishing System (PIPS) starting at an energy of 5 keV and milling angle of 10°. The ion energy and milling angle were gradually brought down to 3 keV and 6° respectively for final polishing and surface cleaning.

The samples were then annealed in flowing dry oxygen at 1050 – 1200 °C for 10 h in a quartz tube furnace. Both samples were baked in air at 300–500 °C for 1–4 h directly before the imaging experiments.

2.2. Imaging experiments

High Resolution TEM (HRTEM) experiments were performed on the TEAM 0.5 instrument (FEI Titan-class) at the National Center for Electron Microscopy (NCEM). The (100) sample with $c(6 \times 2)$ surface reconstruction was imaged at an accelerating voltage of 80 kV with an energy spread of 0.1 eV, 0.2 mrad convergence angle, 1.4 nm defocus spread and the aberration corrector tuned to balance C_3 against the uncorrected residual C_5 ($C_3 = -16 \mu\text{m}$, $C_5 = 6 \text{ mm}$). A focal series of 41 images was acquired at defocus steps of -1.05 nm . The focal series was used for determining the appropriate defocus to maximally enhance bulk subtraction.

The (111) sample with the (3×3) surface reconstruction was imaged at an accelerating voltage of 300 kV with an energy spread of 0.1 eV, 0.15 mrad convergence angle, 0.7 nm focal spread and the aberration corrector tuned to balance C_3 against the uncorrected residual C_5 ($C_3 = -15 \mu\text{m}$, $C_5 = 6 \text{ mm}$). A focal series of 41 images was acquired at defocus steps of -1.72 nm . No significant beam damage was observed in either of the two samples.

2.3. Simulations and post processing

High resolution TEM simulations were performed using MacTempasX Code [78] with experimental parameters and the post processing of both experimental and simulated images (see Supplementary information for the Crystallographic Information File $c(6 \times 2).cif$), bulk removal and correction for top and bottom surface translation, was done using the in house open source code Electron Direct Methods (EDM) [79].

3. Results

High resolution plan view images acquired on two sets of reconstructions on the (001) and (111) surfaces from the same material, SrTiO₃, were subject to image analysis outlined in the methods section. Two model cases, one demonstrating a successful use of the aforementioned method and one a failure, are discussed to present the functionality of the analysis pertaining to two important parameters:

1. Sample thickness, discussed with $c(6 \times 2)$ on SrTiO₃ (001) and the (3×3) on SrTiO₃ (111) as a model cases
2. Symmetry, discussed with (3×3) on SrTiO₃ (111) as a model case

3.1. $c(6 \times 2)$ surface reconstruction on SrTiO₃ (001) surface

High resolution plan view images in a focal series of 41 images were processed using the method outlined in the previous section. The consistency of experimental parameters and defocus were cross checked with simulations from MacTempas. Removal of bulk was done by taking a fast Fourier transform of an image and removing all linear combination of the bulk reciprocal lattice vectors. An unavoidable consequence of this is that the overlapping surface and bulk spots are removed so this is strictly a difference map as mentioned earlier. This was followed by the separation of the top and bottom surface. The resulting image from one of the experimental images acquired at a defocus of 6 Å is given in Fig. 1 along with the corresponding DFT relaxed structure.

In the limits of linear imaging theory, the resulting image can be directly correlated to the intensity of different atomic sites at the surface. The corresponding structure of the $c(6 \times 2)$ surface reconstruction (see Fig. 1) is consistent with atomic resolution secondary electron images [34] as well as x-ray and scanning tunneling microscopy [4] data. The details of the actual structure and surface chemistry are discussed elsewhere [34].

It is evident from Fig. 1 that the method used for the extraction of surface structure is effective. The correlation between the actual structure in Fig. 1b and the relative intensities in the experimental image is strong. The position of Sr atoms appear relatively brighter on the experimental image, consistent with Sr being heavier than Ti and O. Separation performed on all 41 images in the focal series show strong intensity at the Sr position with small modulations in the rest of the image.

Simulations were performed using MacTempas with the structure in Fig. 1(b) (Supplementary information $c(6 \times 2).cif$) for varying bulk thicknesses. The results of the analysis performed at four different thicknesses and hence different bulk contributions and dynamical scattering are given in Fig. 2. Since this method relies on linear imaging theory, there is a critical thickness beyond which the approximations are no longer valid.

Surface signal is highly sensitive to the thickness of the sample. Images simulated at 4.15 nm and 5.32 nm thickness show a strong surface signal evident after bulk subtraction. However, the images simulated at 6.49 nm and 7.66 nm thickness show weak surface

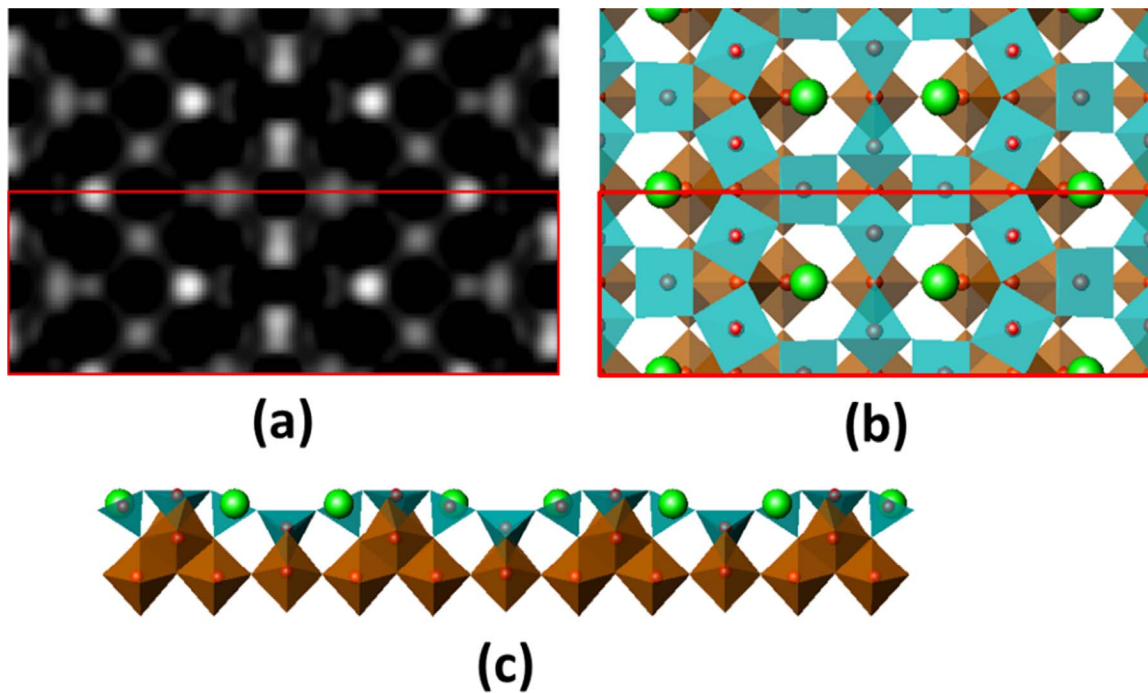


Fig. 1. In (a) experimental image of the $c(6 \times 2)$ surface reconstruction after the removal of bulk and separation of top and bottom surface from high resolution plan view transmission electron microscopy image and the corresponding structure in (b) plan view and (c) profile view. (The unit cell is outlined in red.). (For interpretation of the references to color in this figure legend, the reader is referred to the web version of this article.)

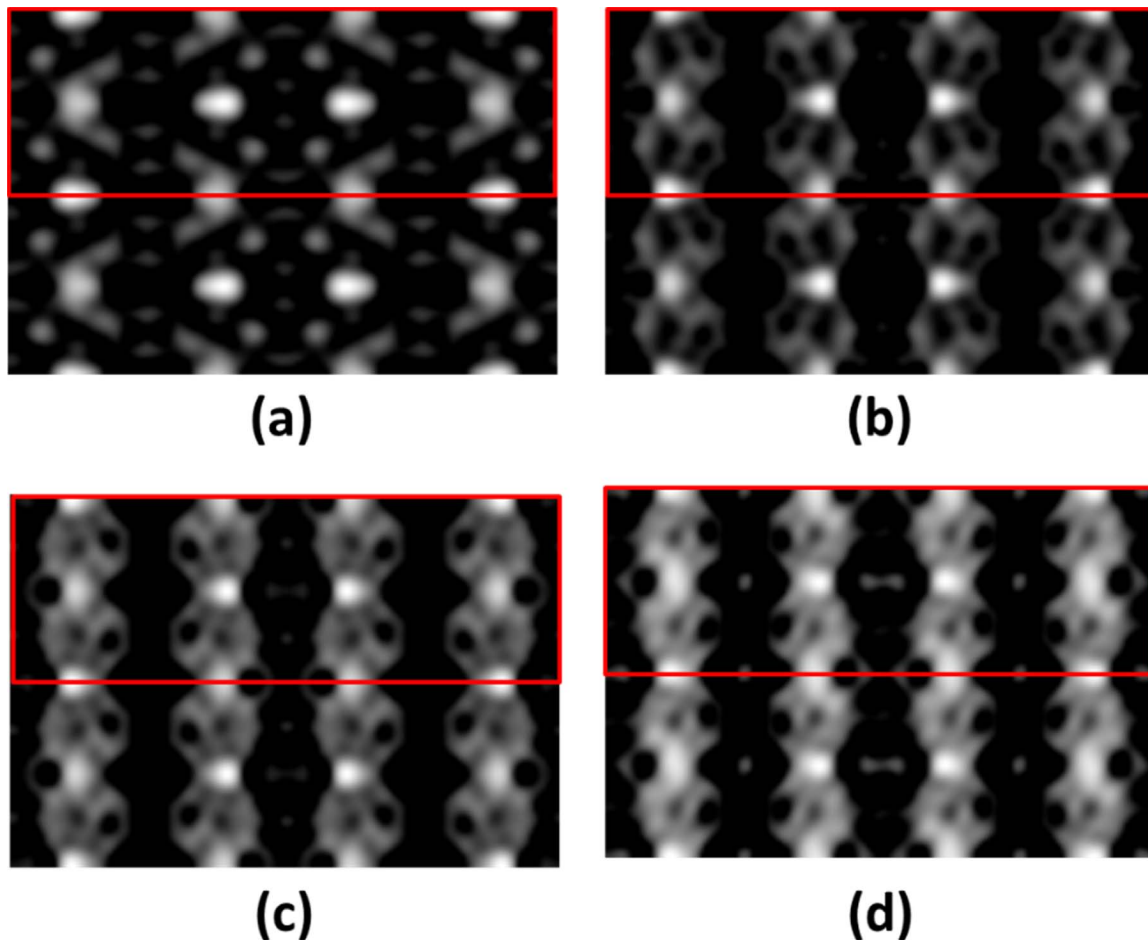


Fig. 2. Simulated plan view images after bulk removal (defocus = 6 Å) at thicknesses of (a) 4.15 nm, (b) 5.32 nm, (c) 6.49 nm and (d) 7.66 nm. Vibration of 0.4 Å (root mean squared) in the x - and y -directions has been added to all images to mimic experimental conditions. (The $c(6 \times 2)$ unit cell is outlined.)

signal. This is a clear demonstration that the thickness of the sample has to be in the kinematical regime, which for the case of SrTiO_3 is approximately 5 nm. The useable, kinematical thickness will vary with respect to the material, orientation, accelerating voltage and aberrations. For instance, the (111) orientation of SrTiO_3 has a higher in plane atomic density than the (100), thus resulting in an even smaller thickness for the kinematical approximation to be valid.

In the case of $c(6 \times 2)$, the presence of an inversion center allows for a more robust separation of the top and bottom surface unlike in the case of the (3×3) surface reconstruction on SrTiO_3 (111) surface. This in large part is because the phase can only be 0 or 180 degrees with inversion symmetry. It is worth remembering that the phase is generally more important than the amplitude in obtaining representative images.

3.2. (3×3) surface reconstruction on SrTiO_3 (111)

The separation of the top and bottom surface was done in two different plane group symmetries: $p6mm$ and $p3m1$. While the actual structure is $p3m1$, the lack of inversion symmetry in $p3m1$ makes it difficult to interpret the resulting image. We note that it is well established with direct methods of inverting diffraction data that sometimes higher symmetry space groups with

inversion symmetry solve better, particularly if the symmetry reduction of the true structure is small; this was also found for surfaces [74].

Separation of the top and bottom surface was performed on the same experimental image taken at a defocus of 5.4 nm. The resulting images in $p6mm$ and $p3m1$ after the separation are given in Figs. 3a and b, respectively. One common feature that is consistent across both the images is the high signal at the origin. In contrast, other experimental data including STM and density functional theory based calculations [80] (see Figs. 3c and d) show the opposite. This can be attributed to relatively thick samples, thicker than the sample on which the $c(6 \times 2)$ was observed. As seen in Fig. 2, the restrictions on the thickness of the sample is strict and the higher in plane atomic density along (111) in comparison to the (001) direction is detrimental to the validity of kinematical assumptions.

In addition to the inconsistency at the origin, the $p3m1$ image in general does not match with the experimental STM image making it almost impossible to interpret the contrast or the atomic positions. On the contrary, the image in $p6mm$ provides significant details that are consistent with the STM image and the structure. However, since the actual structure is not $p6mm$ the intensities are deviant. The six membered ring at the origin is rotated by 30° . However, besides the rotation of the six membered ring and

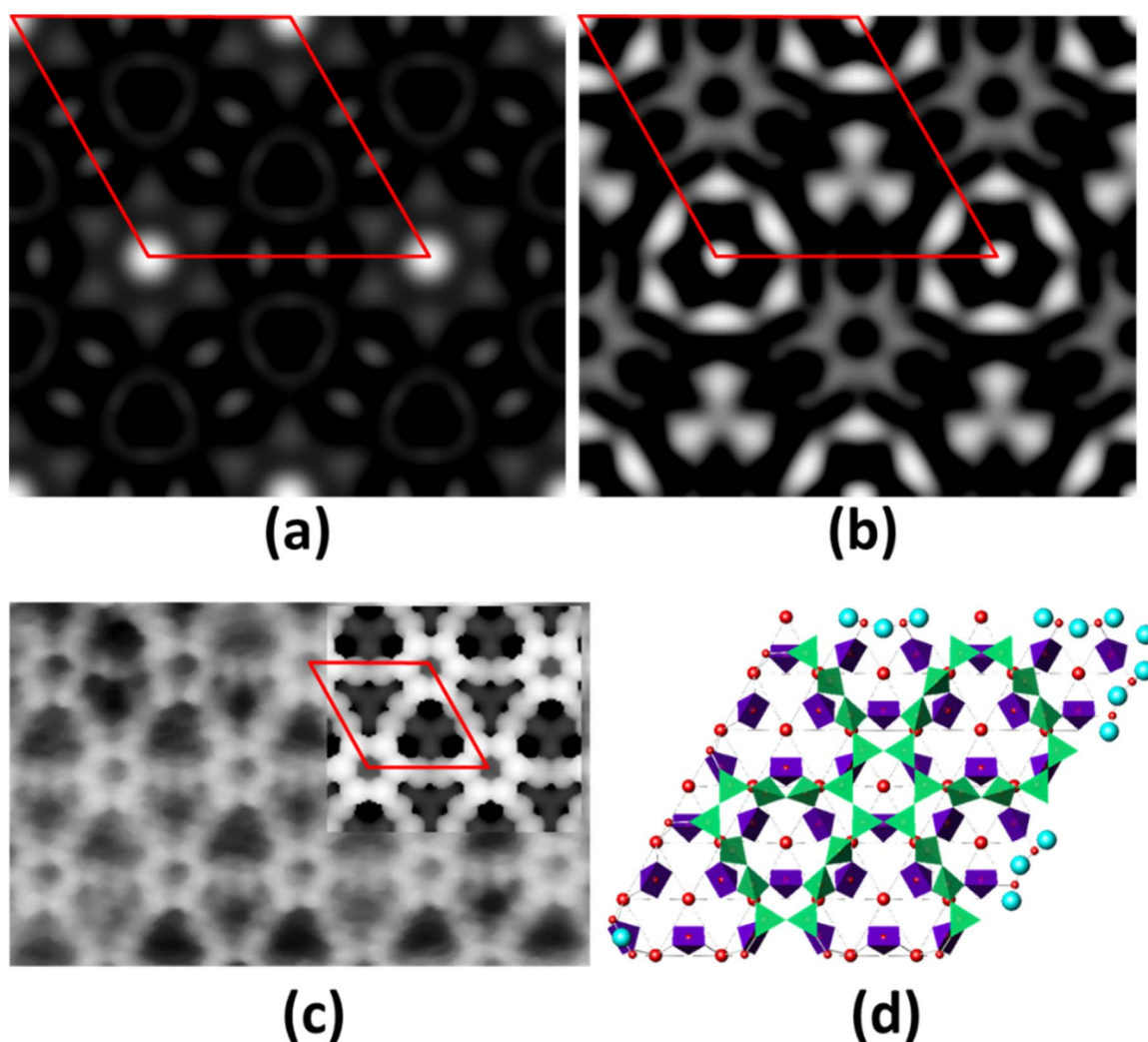


Fig. 3. Experimental HREM image in (a) with $p6mm$ symmetry and in (b) with $p3m1$ symmetry used for the separation of top and bottom surface after bulk removal. In (c) STM image with the simulation overlaid and (d) the corresponding structure of the (3×3) surface reconstruction on SrTiO_3 on (111) [Subfigures (c) and (d) adapted from Ref. [80].] (The (3×3) unit cell is outlined in red.). (For interpretation of the references to color in this figure legend, the reader is referred to the web version of this article.)

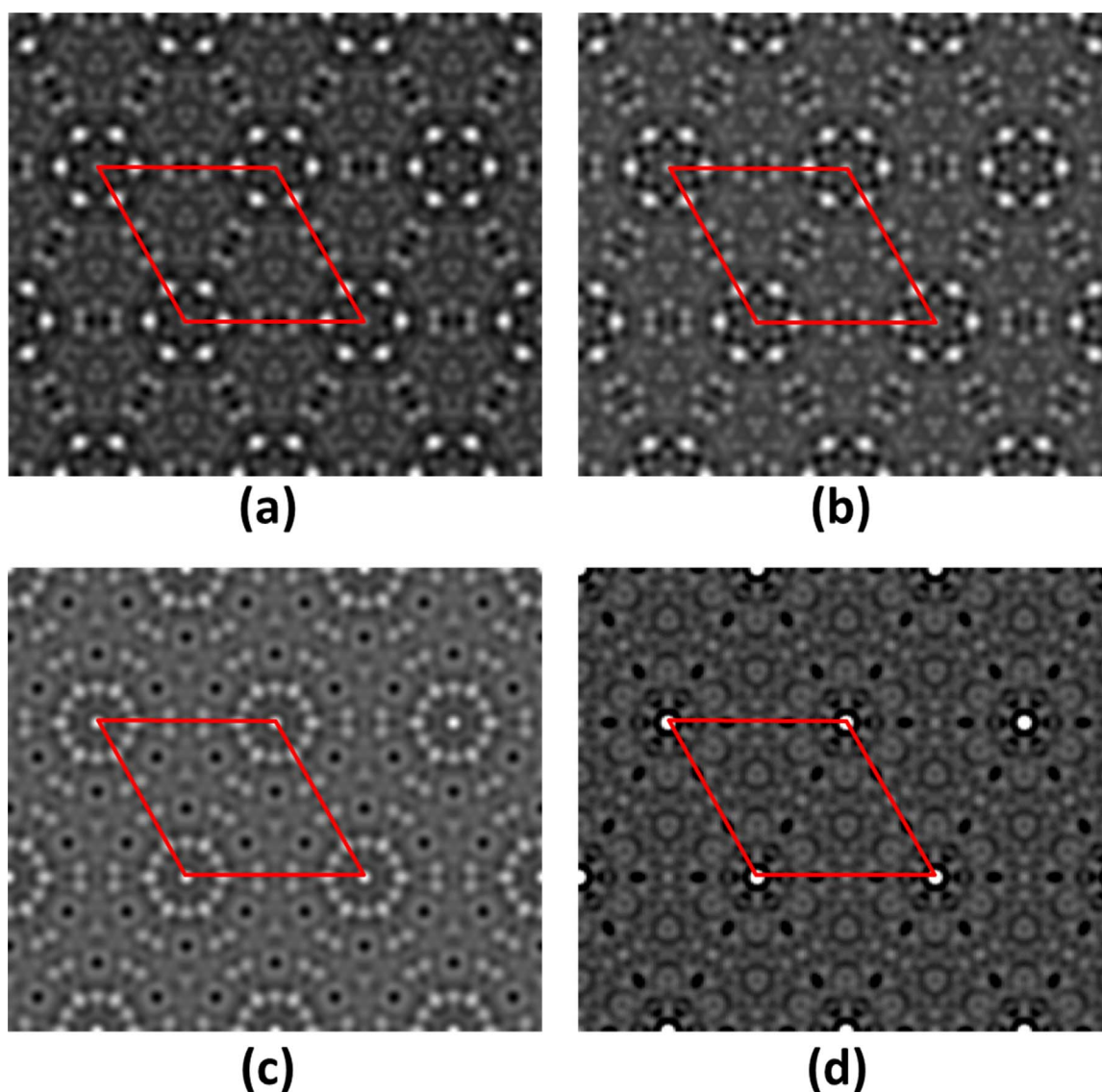


Fig. 4. Simulated HREM images of the (3×3) surface reconstruction on SrTiO_3 (111) after bulk removal at varying thicknesses in (a) 5 nm, (b) 6.33 nm, (c) 7.7 nm and (d) 9.07 nm. (The (3×3) surface unit cell is outlined in red.). (For interpretation of the references to color in this figure legend, the reader is referred to the web version of this article.)

strong intensity at the origin, the $p6mm$ image provides a better match with the experimental image, thus demonstrating the importance of an inversion center.

This was validated with HREM simulations performed on the (3×3) . The simulations were performed with $S3 \times 3.cif$ (see [Supplemental materials](#)) using the experimental parameters given in the methods section (Figs. 4 and 5).

The high intensity observed at the origin in the experimental plan view images is only seen in simulated images of at least 6 nm thickness (Fig. 4); the intensity at the origin increases with thickness. Hence, the high intensity at the origin observed in the experimental image is the result of dynamical effects in thicker sample. In addition, the rotation of the six membered ring is not present in the simulated image below a thickness of 6 nm. However, the image simulated at 7.7 nm thickness starts to show intensity that is consistent with the 30° rotation of the hexagonal ring. Finally, the image simulated at a thickness of 9.07 nm shows the rotation of the six membered ring consistent with the inversion performed on experimental images. This further validates that the sample in the case of (3×3) was in the tens of nm.

For completeness, experimental images on the two extremes of

the focal series were also analyzed to compare the separation under $p6mm$ and $p3m1$ (Fig. 5). This is particularly important if there is inversion of phases during the separation and in some cases the resulting solution could be an example of Babinet's principle, i.e. the inverse solution. The contrast on the two ends of the focal spectrum clearly demonstrate that the intensities are still consistent in $p6mm$. However, in the case of $p3m1$ there is a dramatic change in contrast. This can also be attributed to the presence of inversion center in $p6mm$ which makes the intensities symmetric on both sides of the focal series.

4. Discussion

The primary limitation of the inversion method lies in the assumption that the scattering is in the kinematical regime which as we have seen in the case of the (3×3) is not always valid. Implementation of dynamical scattering theory would be essential going beyond surface structures with inversion symmetry or a thin sample.; while this has been done to refine surface diffraction data (e.g. [44,81–83]), it is rather tedious and it is unclear how to do

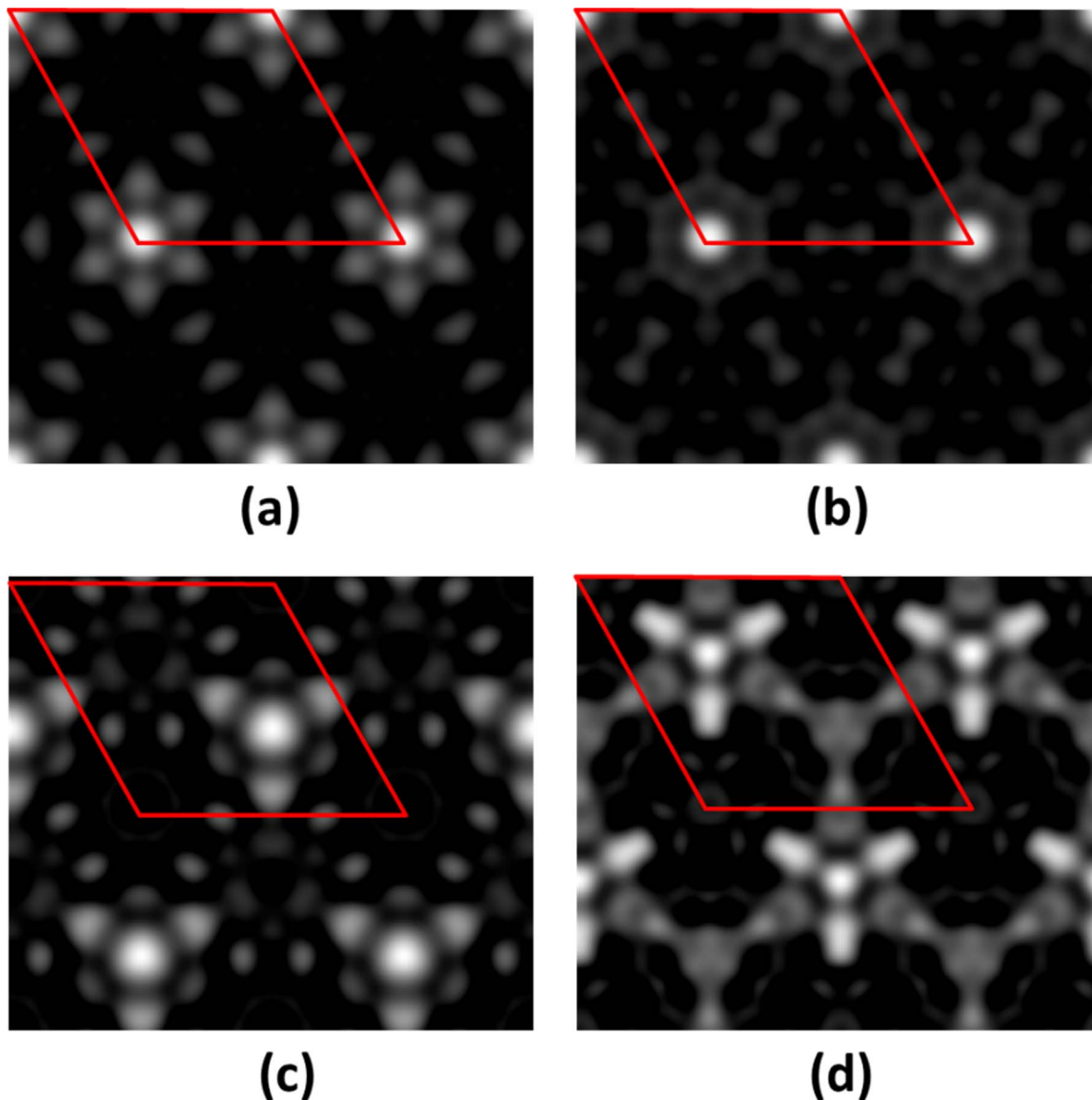


Fig. 5. Experimental images after bulk removal and separation of top and bottom surface: with $p6mm$ symmetry in (a) and (b) with defocus of experimental image at 41.3 nm and -27.5 nm respectively and with $p3m1$ symmetry in (c) and (d) with defocus of experimental image at 41.3 nm and -27.5 nm respectively.

this simply. Another challenge would be to account for differences in the top and bottom surface. There can be coexisting domains as well as different overlapping periodicities. While the inversion may still work if the surface structure of concern occupies a majority of the surface area as the plan view method works with the average of domains, this is not always the case. This gives rise to inconsistency in the results even for images acquired from the same sample but from different areas. For instance, different $(n \times n)$ reconstructions have been found to coexist on the SrTiO_3 (111) surface along with other difficulties due to long range disorder in the sample and glass like behavior of some of the surfaces [80]. Similarly, issues with the signal to noise (S/N) ratio from the surface is critical. It could well be that beyond a certain thickness, the S/N from the surface is insufficient for extracting any useful information.

Plan view imaging possesses good surface signal, 1–3% of the total signal, if the sample is thin. This method has been used for four systems, (7×7) on silicon (111) [41], 5×2 -Au on silicon (111) [46], 2×1 on SrTiO_3 [26] and $c(6 \times 2)$ on SrTiO_3 (001) [34], successfully. However, there are restrictions, the first being on the thickness of the sample. The second requirement which is subtler

pertains to having inversion symmetry. The requirements for inversion symmetry can be thought of as imposing restriction on the sets of phases for different reflections thus making the method more robust and the resulting intensities more reliable. Thus, plan view imaging on the zone axis is a powerful tool when applied to imaging surface structures with proper address to the limitations and functionality of the method. An alternative is to tilt off the zone axis which will reduce dynamical effects, but introduces additional issues as the signal is weaker [50].

Acknowledgment

PK acknowledges funding by the Department of Energy on Grant number DE-FG02-01ER45945. Electron microscopy was performed at the Molecular Foundry at Lawrence Berkeley National Lab, which is supported by the Office of Basic Energy Sciences of the US Department of Energy under Contract no. DE-AC02-05CH11231.

Appendix A. Supplementary material

Supplementary data associated with this article can be found in the online version at <http://dx.doi.org/10.1016/j.ultramic.2016.08.001>.

References

- J.E.T. Andersen, P.J. Møller, Impurity-induced 900 °C (2×2) surface reconstruction of SrTiO₃(100), *Appl. Phys. Lett.* 56 (1990) 1847.
- Y. Cao, S. Wang, S. Liu, Q. Guo, J. Guo, Electronic structures of the SrTiO₃(110) surface in different reconstructions, *J. Chem. Phys.* 137 (2012) 044701.
- M.S. Gonzalez, M.H. Aguirre, E. Mora, M.C. Asensio, In situ reduction of (100) SrTiO₃, *Solid State Sci.* 2 (2000) 519–524.
- D. Jiang, J. Zegenhagen, $c(6 \times 2)$ and $c(4 \times 2)$ reconstructions of the SrTiO₃(001), *Surf. Sci.* 425 (1999) 343–354.
- P.J. Møller, A. Komolov, F. Lazneva, Selective growth of a MgO (100) $c(2 \times 2)$ superstructure on a SrTiO₃ (100)– (2×2) substrate, *Surf. Sci.* 425 (1999) 15–21.
- R. Shimizu, K. Iwaya, T. Ohsawa, S. Shiraki, T. Hasegawa, T. Hashizume, T. Hitosugi, Effect of oxygen deficiency on SrTiO₃ (001) surface reconstructions, *Appl. Phys. Lett.* 100 (2012) 263106.
- T. Beck, A. Klust, M. Batzill, U. Diebold, C. Di Valentin, A. Selloni, Surface structure of TiO₂(011)– (2×1) , *Phys. Rev. Lett.* 93 (2004) 036104.
- M.R. Castell, Nanostructures on the SrTiO₃ (001) surface studied by STM, *Surf. Sci.* 516 (2002) 33–42.
- M.R. Castell, Scanning tunneling microscopy of reconstructions on the SrTiO₃(001) surface, *Surf. Sci.* 505 (2002) 1–13.
- D.S. Deak, F. Silly, D.T. Newell, M.R. Castell, Ordering of TiO₂-based nanostructures on SrTiO₃(001) surfaces, *J. Phys. Chem. B* 110 (2006) 9246–9251.
- D.S. Deak, F. Silly, K. Porfyriakis, M.R. Castell, Controlled surface ordering of endohedral fullerenes with a SrTiO₃ template, *Nanotechnology* 18 (2007) 075301.
- J. Feng, X. Zhu, J. Guo, Reconstructions on SrTiO₃(111) surface tuned by Ti/Sr deposition, *Surf. Sci.* 614 (2013) 38–45.
- K. Johnston, M. Castell, A. Paxton, M. Finnis, SrTiO₃(001) (2×1) reconstructions: first-principles calculations of surface energy and atomic structure compared with scanning tunneling microscopy images, *Phys. Rev. B* 70 (2004) 085415.
- T. Kubo, H. Nozoye, Surface structure of SrTiO₃(100), *Surf. Sci.* 542 (2003) 177–191.
- T. Kubo, H. Nozoye, Surface Structure of SrTiO₃(100)– $(\sqrt{5} \times \sqrt{5})$ -R26.6°, *Phys. Rev. Lett.* 86 (2001) 1801–1804.
- Y. Lin, A.E. Becerra-Toledo, F. Silly, K.R. Poeppelmeier, M.R. Castell, L.D. Marks, The (2×2) reconstructions on the SrTiO₃ (001) surface: a combined scanning tunneling microscopy and density functional theory study, *Surf. Sci.* 605 (2011) L51–L55.
- L.D. Marks, aN. Chiaramonti, S.U. Rahman, M.R. Castell, Transition from order to configurational disorder for surface reconstructions on SrTiO₃ (111), *Phys. Rev. Lett.* 114 (2015) 1–6.
- H.L. Marsh, D.S. Deak, F. Silly, al. Kirkland, M.R. Castell, Hot STM of nanostructure dynamics on SrTiO₃ (001), *Nanotechnology* 17 (2006) 3543–3548.
- D. Newell, A. Harrison, F. Silly, M. Castell, SrTiO₃(001)– (5×5) -R26.6° reconstruction: a surface resulting from phase separation in a reducing environment, *Phys. Rev. B* 75 (2007) 205429.
- T. Ohsawa, K. Iwaya, R. Shimizu, T. Hashizume, T. Hitosugi, Thickness-dependent local surface electronic structures of homoepitaxial SrTiO₃ thin films, *J. Appl. Phys.* 108 (2010) 073710.
- B.C. Russell, M.R. Castell, Surface of sputtered and annealed polar SrTiO₃ (111): TiO₂-rich $(n \times n)$ reconstructions, *J. Phys. Chem. C* 3 (2008) 6538–6545.
- B. Russell, M. Castell, $(\sqrt{13} \times \sqrt{13})R13.9^\circ$ and $(\sqrt{7} \times \sqrt{7})R19.1^\circ$ reconstructions of the polar SrTiO₃(111) surface, *Phys. Rev. B* 75 (2007) 155433.
- F. Silly, D.T. Newell, M.R. Castell, SrTiO₃ (001) reconstructions: the (2×2) to $c(4 \times 4)$ transition, *Surf. Sci.* 600 (2006) L219–L223.
- A.N. Chiaramonti, C.H. Lanier, L.D. Marks, P.C. Stair, Time, temperature, and oxygen partial pressure-dependent surface reconstructions on SrTiO₃(111): a systematic study of oxygen-rich conditions, *Surf. Sci.* 602 (2008) 3018–3025.
- S. Gerhold, Z. Wang, M. Schmid, U. Diebold, Stoichiometry-driven switching between surface reconstructions on SrTiO₃(001), *Surf. Sci.* 621 (2014) L1–L4.
- N. Erdman, K.R. Poeppelmeier, M. Asta, O. Warschkow, D.E. Ellis, L.D. Marks, The structure and chemistry of the TiO₂-rich surface of SrTiO₃ (001), *Nature* 419 (2002) 55–58.
- N. Erdman, O. Warschkow, M. Asta, K.R. Poeppelmeier, D.E. Ellis, L.D. Marks, Surface structures of SrTiO₃ (001): a TiO₂-rich reconstruction with a $c(4 \times 2)$ unit cell, *J. Am. Chem. Soc.* 125 (2003) 10050–10056.
- D.M. Kienzie, aE. Becerra-Toledo, L.D. Marks, Vacant-site octahedral tilings on SrTiO₃ (001), the $(\sqrt{13} \times \sqrt{13})R33.7^\circ$ surface, and related structures, *Phys. Rev. Lett.* 106 (2011) 176102.
- C. Lanier, A. van de Walle, N. Erdman, E. Landree, O. Warschkow, A. Kazimirov, K. Poeppelmeier, J. Zegenhagen, M. Asta, L. Marks, Atomic-scale structure of the SrTiO₃(001)– $c(6 \times 2)$ reconstruction: experiments and first-principles calculations, *Phys. Rev. B* 76 (2007) 045421.
- A. Pancotti, N. Barrett, L.F. Zagonel, G.M. Vanacore, Multiple scattering x-ray photoelectron diffraction study of the SrTiO₃(100) surface, *J. Appl. Phys.* 106 (2009) 034104.
- O. Bunk, G. Falkenberg, J.H. Zeysing, L. Lottermoser, R.L. Johnson, Structure determination of the indium-induced Si(111)– (4×1) reconstruction by surface x-ray diffraction, *Phys. Rev. B* 59 (1999) 12228–12231.
- J. Cheng, P. Regreny, L. Largeau, G. Patriarche, O. Mauguin, K. Naji, G. Hollinger, G. Saint-Giron, Influence of the surface reconstruction on the growth of InP on SrTiO₃(001), *J. Cryst. Growth* 311 (2009) 1042–1045.
- M. Naito, H. Sato, Reflection high-energy electron diffraction study on the SrTiO₃ surface structure, *Physica C* 229 (1994) 1–11.
- J. Ciston, H.G. Brown, aj, D'Alfonso, P. Koirala, C. Ophus, Y. Lin, Y. Suzuki, H. Inada, Y. Zhu, L.J. Allen, L.D. Marks, Surface determination through atomically resolved secondary-electron imaging, *Nat. Commun.* 6 (2015) 7358.
- F. Bottin, F. Finocchi, C. Noguera, Faceting and $(n \times 1)$ reconstructions of SrTiO₃(110) surfaces, *Surf. Sci.* 574 (2005) 65–76.
- S.-H. Phark, Y.J. Chang, T. Won Noh, Selective growth of perovskite oxides on SrTiO₃ (001) by control of surface reconstructions, *Appl. Phys. Lett.* 98 (2011) 161908.
- O. Warschkow, M. Asta, N. Erdman, K.R. Poeppelmeier, D.E. Ellis, L.D. Marks, TiO₂-rich reconstructions of SrTiO₃(001): a theoretical study of structural patterns, *Surf. Sci.* 573 (2004) 446–456.
- S.N. Klimin, J. Tempere, J.T. Devreese, D. van der Marel, Interface superconductivity in LaAlO₃–SrTiO₃ heterostructures, *Phys. Rev. B* 89 (2014) 184514.
- A. Ohtomo, H.Y. Hwang, A high-mobility electron gas at the LaAlO₃/SrTiO₃ heterointerface, *Nature* 427 (2004) 423–426.
- D.N. Dunn, P. Xu, L.D. Marks, UHV transmission electron microscopy of Ir (001) I. Microstructure of the (1×1) and the reconstructed (5×1) surfaces, *Surf. Sci.* 294 (1993) 308–321.
- E. Bengu, R. Plass, L. Marks, T. Ichihashi, P. Ajayan, S. Iijima, Imaging the Dimers in Si(111)– (7×7) , *Phys. Rev. Lett.* 77 (1996) 4226–4228.
- S. Li, R. Li, R. Guan, H. Ye, J. Zhu, Plan-view imaging of oxygen-induced reconstruction on Ag(110) surface. I. The possibility of imaging surface oxygen, *J. Electron Microsc.* 49 (2000) 163–172.
- L.D. Marks, Registry and UHV transmission electron diffraction of surfaces, *Ultramicroscopy* 45 (1992) 145–154.
- L.D. Marks, P. Xu, D.N. Dunn, UHV transmission electron-microscopy of Ir(001) II. atomic positions of the (5×1) reconstructed surface from HREM and R-factor refinements, *Surf. Sci.* 294 (1993) 322–332.
- L.D. Marks, Rigor, and plan-view simulation of surfaces, *Ultramicroscopy* 38 (1991) 325–332.
- L.D. Marks, R. Plass, Atomic structure of Si(111)– (5×2) -Au from high resolution electron microscopy and heavy-atom holography, *Phys. Rev. Lett.* 75 (1995) 2172–2175.
- P. Xu, L.D. Marks, Intensities of surface diffraction spots in plan view, *Ultramicroscopy* 45 (1992) 155–157.
- N. Ikarashi, K. Kobayashi, H. Koike, H. Hasegawa, K. Yagi, Profile and plan-view imaging of reconstructed surface structures of gold, *Ultramicroscopy* 26 (1988) 195–203.
- M.A. Gribelyuk, P.J.F. Harris, J.L. Hutchison, Plan-view and profile imaging of sulphided platinum particles, *Philos. Mag. Part B* 69 (1994) 655–669.
- P. Xu, D. Dunn, J.P. Zhang, L.D. Marks, Atomic imaging of surfaces in plan view, *Surf. Sci.* 285 (1993) L479–L485.
- L.D. Marks, Direct atomic imaging of solid surfaces I. Image simulation and interpretation, *Surf. Sci.* 139 (1984) 281–298.
- L.D. Marks, D.J. Smith, Direct atomic imaging of solid surfaces II. Gold (111) surfaces during and after in situ carbon etching, *Surf. Sci.* 143 (1984) 495–508.
- D.J. Smith, L.D. Marks, Direct atomic imaging of solid surfaces III. Small particles and extended Au surfaces, *Ultramicroscopy* 16 (1985) 101–114.
- L.D. Marks, D.J. Smith, Direct atomic imaging of solid surfaces IV. Dislocations on Au(100), *Surf. Sci. Lett.* 157 (1985) 367–372.
- L.D. Marks, Direct imaging of carbon-covered and clean gold (110) Surfaces, *Phys. Rev. Lett.* 51 (1983) 1000–1002.
- D.J. Smith, L.D. Marks, Direct lattice imaging of small metal particles, *Philos. Mag.* 44 (1981) 735–740.
- L.D. Marks, V. Heine, D.J. Smith, Direct observation of elastic and plastic deformations at the Au(111) surfaces, *Phys. Rev. Lett.* 52 (1984) 656–658.
- L.D. Marks, D.J. Smith, Direct surface imaging in small metal particles, *Nature* 303 (1983) 316–317.
- L.D. Marks, D.J. Smith, High resolution studies of small particles of gold and silver I. Multiply-twinned particles, *J. Cryst. Growth* 54 (1981) 425–432.
- D. Smith, L. Marks, High resolution studies of small particles of gold and silver: II. Single crystals, lamellar twins and polyparticles, *J. Cryst. Growth* 54 (1981) 433–438.
- L.D. Marks, A. Howie, Multiply-twinned particles in silver catalysts, *Nature* 282 (1979) 196–198.
- A. Howie, L.D. Marks, S.J. Pennycook, New imaging methods for catalyst particles, *Ultramicroscopy* 8 (1982) 163–174.
- L.D. Marks, Surface structure and energetics of multiply twinned particles, *Philos. Mag.* 49 (1984) 81–93.
- Y. Lin, Z. Wu, J. Wen, L. Hu, R.M. Kennedy, P.C. Stair, K.R. Poeppelmeier, L.D. Marks, Synthesis-dependent atomic surface structures of oxide nanoparticles, *Phys. Rev. Lett.* 111 (2013) 156101.
- Y. Lin, Z. Wu, J. Wen, K.R. Poeppelmeier, L.D. Marks, Imaging the atomic surface structures of CeO₂ Nanoparticles, *Nano Lett.* 14 (2014) 191–196.
- J.L. Hutchison, N.A. Briscoe, Surface profile imaging of spinel catalyst particles, *Ultramicroscopy* 18 (1985) 435–438.

- [67] A.K. Datye, D.J. Smith, The study of heterogeneous catalysts by high-resolution transmission electron microscopy, *Catal. Rev.* 34 (1992) 129–178.
- [68] L.C. Gontard, L.Y. Chang, C.J. Hetherington, A.I. Kirkland, D. Ozkaya, R.E. Dunin-Borkowski, Aberration-corrected imaging of active sites on industrial catalyst nanoparticles, *Angew. Chem Int Ed. Engl.* 46 (2007) 3683–3685.
- [69] P.L. Hansen, J.B. Wagner, S. Helveg, J.R. Rostrup-Nielsen, B.S. Clausen, H. Topsøe, Atom-resolved imaging of dynamic shape changes in supported copper nanocrystals, *Science* 295 (2002) 2053–2055.
- [70] D.A. Jefferson, P.J.F. Harris, Direct imaging of an adsorbed layer by high-resolution electron microscopy, *Nature* 332 (1988) 617–620.
- [71] J.O. Bovin, R. Wallenberg, D.J. Smith, Imaging of atomic clouds outside the surfaces of gold crystals by electron microscopy, *Nature* 317 (1985) 47–49.
- [72] Y. Lin, J. Wen, L. Hu, R.M. Kennedy, P.C. Stair, K.R. Poeppelmeier, L.D. Marks, Synthesis-dependent atomic surface structures of oxide nanoparticles, *Phys. Rev. Lett.* 111 (2013) 1–5.
- [73] Y. Lin, Z. Wu, J. Wen, K.R. Poeppelmeier, L.D. Marks, Imaging the atomic surface structures of CeO₂ nanoparticles, *Nano Lett.* 2 (2014).
- [74] C.J. Gilmore, L.D. Marks, D. Grozea, C. Collazo, E. Landree, R.D. Twisten, Direct solutions of the Si(111) 7x7 structure, *Surf. Sci.* 381 (1997) 77–91.
- [75] L.D. Marks, Rigor, and plan-view simulation of surfaces, *Ultramicroscopy* 38 (1991) 325–332.
- [76] L.D. Marks, T.S. Savage, J.P. Zhang, R. Ai, Validity of the kinematical approximation in transmission electron-diffraction for surfaces, revisited, *Ultramicroscopy* 38 (1991) 343–347.
- [77] L.D. Marks, Registry and UHV transmission electron diffraction of surfaces, *Ultramicroscopy* 45 (1992) 145–154.
- [78] R. Kilaas, *MacTempasX*, in, 2015.
- [79] R. Kilaas, L.D. Marks, C.S. Own, EDM 1.0: electron direct methods, *Ultramicroscopy* 102 (2005) 233–237.
- [80] L.D. Marks, A.N. Chiamonti, S.U. Rahman, M.R. Castell, Transition from order to configurational disorder for surface reconstructions on SrTiO₃(111), *Phys. Rev. Lett.* 114 (2015) 226101.
- [81] R. Plass, L.D. Marks, UHV transmission electron-microscopy structure determination of the Si(111)-(√3 × √3)-R30°-Au surface, *Surf. Sci.* 342 (1995) 233–249.
- [82] C. Collazo-Davila, D. Grozea, E. Landree, L.D. Marks, Transmission electron diffraction determination of the Ge(001)-(2 × 1) surface structure, *Surf. Sci.* 375 (1997) 293–301.
- [83] C. Collazo-Davila, D. Grozea, L.D. Marks, Determination and refinement of the Ag/Si(111)-(3 × 1) surface structure, *Phys. Rev. Lett.* 80 (1998) 1678–1681.